Zaria Journal of Electrical Engineering Technology, Department of Electrical Engineering, Ahmadu Bello University, Zaria - Nigeria. Vol. 13 No. 1 & 2, September 2024.

Subthreshold Signal Enhancement in a Space-Dependent Damped Van der Pol-Duffing Oscillator via Vibrational Resonance

Usama Bello Ibrahim[1], Hamza Mustapha[2], Mannir Ahmad[3], Adamu Saidu Abubakar[2]

[1]Department of Physics, Aliko Dangote University of Science and Technology, Wudil, Kano-Nigeria.

[2]Department of Electrical Engineering, Ahmadu Bello University Zaria, Nigeria.

[3]Department of Electrical Engineering, Aliko Dangote University of Science and Technology Wudil, Kano-Nigeria.

*usamabelloibrahim@kustwudil.edu.ng

Keywords: –
Subthreshold signal
Signal enhancement
Van der Pol oscillator
Space-dependent damping
Vibrational Resonance

Article History: – Received: Dec. 22, 2023
Reviewed: Feb. 5, 2024
Accepted: Feb. 17, 2024
Published: Mar. 19, 2024

ABSTRACT

This paper presents a numerical study of a subthreshold signal enhancement in a Van der Pol-Duffing oscillator, via the phenomenon of vibrational resonance. The oscillator describes a particle motion in a bistable periodic potential, influenced by space-dependent damping and excited by an external bichromatic excitation. Temporal and spectral analyses approaches were employed to analyze the system response. The analyses revealed that the input low frequency signal is enhanced when the amplitude of high frequency perturbation tuned to an intermediate value. This result is also highlighted in the linear response analysis for fixed value of the damping amplitude. Moreover, the damping amplitude is found to control the system's response. However, the best response $Q = 7.01557$is achieved for an intermediate value of the damping amplitude $\gamma = 0.05$.

1. INTRODUCTION

The fascinating ubiquitous nature of nonlinear systems has drawn the interest of many researchers for decades. Consequently, diverse dynamical properties have been examined theoretically, numerically and experimentally in nonlinear systems. Among the most investigated dynamical behaviors is undoubtedly resonance-induced phenomena which include; chaotic resonance [1], coherence resonance [2-6], stochastic resonance [7]-[13], vibrational resonance [14-18] and ghost resonance [17], [19]-[22], to mention few. Among the resonance-induced behaviors in nonlinear systems, more attention has been devoted to the famous Stochastic Resonance (SR) and Vibrational Resonance (VR).

Stochastic Resonance (SR) is a noise-induced phenomenon where the detection of a low- frequency input signal at the output of nonlinear system is improved due to the presence of noise perturbation. SR phenomenon has been investigated by researchers from different fields for more than three decades now, and it has been reported to have a lot of applications in signal detection [23], [24], image perception [25], [26] and signal/information transmission [27], [28]. On the other hand, the ultimate VR, unlike SR, is deterministic. Nonlinear systems improve their output response at the low frequency due to presence of high frequency perturbation. VR is deterministic and easy to handle unlike SR which is stochastic. Since its first discovery by Landa and McClintock in bistable systems

[14], Vibrational Resonance (VR) has been investigated in many systems and in different context [29]-[33].

Recently, VR has been investigated in different mechanical models. Particularly, the impact of positions and shapes of the potential well on VR occurrence has been investigated [34], [35]. Moreover, the effects of the nature of damping and the damping parameters on VR occurrence have been investigated in many mechanical systems [36], [37]. However, few research works focused on the impact of space-dependent damping parameters on VR occurrence [31, 38]. T. O. Roy-Layinde *et al* [31] and B. I. Usama *et al* [38] have investigated the effect of space-dependent damping parameters on VR occurrence in a harmonic oscillator. Their studies both reported that, the parameters of the space-dependent damping can be used to control the system's response and also to enhance its performance. In this paper, the impact of damping parameter on VR occurrence in a space-dependent damped Van der Pol-Duffing oscillator was investigated and to the best of our knowledge has not been investigated by any researcher.

The rest of the article is arranged as follows: section 2 introduced detailed model of the system, section 3 provides detailed methodology of the research, section 4 studied response of the system by using temporal, spectral and linear response analyses, and section 5 concludes the finding of the research.

2. THE MODEL

The system considered in this work is a variant of Van der Pol-Duffing oscillator which models the motion of a single particle of mass m in a bistable potential well $\Phi(x)$, damped by a space-dependent periodic force and driven by an external bichromatic excitation $e(t)$.

$$m\frac{d^2x}{dt^2} + \frac{d\Phi(x)}{dx} + \gamma(x)\frac{dx}{dt} = e(t) \qquad (1)$$

The bistable potential $\Phi(x)$ is defined by the relation

$$\Phi(x) = \frac{\alpha}{4}x^4 - \frac{1}{2}\omega_0^2x^2 \qquad (2)$$

where the parameters α and ω_0 adjust the width and potential barrier. Figure 1 depicts the system's potential for $\alpha = 0.19$ and $\omega_0 = 1$. The particle has two equilibrium positions located at $x = -2.29$ and $x = +2.29$ for the given parameter set. For the particle to jump from one equilibrium position to the other it has overcome the potential barrier $\Delta\Phi$.

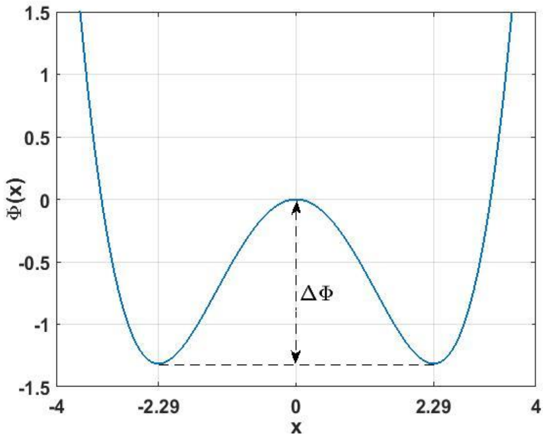

Fig. 1: The system's bistable potential defined by equation (2) for α=0.19 and ω_0=1.

The system is damped with a parametrically excited damping. The parametric damping coefficient $\gamma(x)$ is defined as;

$$\gamma(x) = \gamma\left(1 + h\cos\omega_p x\right)(x^2 - 1) \qquad (3)$$

The damping coefficient is periodic with amplitude h and frequency ω_p. The parameter γ is the whole amplitude of the damping which if set to zero, the system becomes undamped. Somnath Roy *et al* [39] considered this model defined by equation (1), but with time-dependent damping, equation (1) becomes: $\gamma(\boldsymbol{t}) = \gamma\big(1 + h\cos\omega_p \boldsymbol{t}\big)(x^2 - 1)$ to control the occurrence of subharmonic resonance and chaos.

Lastly, the system is excited by two set of signals; low frequency signal $(F\cos\omega t)$ mixed with a high frequency perturbation $(G\cos\Omega t)$. The excitation $e(t)$ is given as;

$$e(t) = F\cos\omega t + G\cos\Omega t \qquad (4)$$

Thus, the complete model of the system can be rewritten as;

$$m\frac{d^2x}{dt^2} + (\alpha x^3 - \omega_0^2 x) + \left(\gamma\big(1 + h\cos\omega_p x\big)(x^2 - 1)\right)\frac{dx}{dt} = F\cos\omega t + G\cos\Omega t \qquad (5)$$

3. METHODOLOGY

In this article, fourth order Runge-Kutta algorithm is employed in MATLAB to numerically integrate the system defined by equation (5). This is done by first converting our system defined by equation (5) into set of two first order differential equations;

$$\begin{cases} \frac{dx}{dt} = y, \\ \frac{dy}{dt} = \left(-\frac{d\Phi(x)}{dx} - \gamma(x)y + F\cos\omega t + G\cos\Omega t\right)\Big/ m \end{cases} \qquad (6)$$

Runge-Kutta algorithm with 2000 low frequency drive cycles, 2^{22} total number of samples and step size $dt = \left(\frac{2000}{2^{22}}\right)\frac{2\pi}{\omega}$ is considered. The corresponding spectral resolution is therefore $df = \frac{1}{Ndt}$. The simulation result is basically the output signal $x(t)$ obtained for a range of time t. The corresponding output spectra $X(f)$ is obtained by computing the Fast Fourier Transform (FFT) of the output signal $x(t)$

$$X(f) = fft\big(x(t)\big) \qquad (7)$$

The output spectra obtained from MATLAB software is bilateral and complex therefore, the required unilateral magnitude spectrum is $2|X(f)|$. The output unilateral magnitude spectra $2|X(f)|$ contain both the low frequency $\frac{\omega}{2\pi}$ and the high frequency $\frac{\Omega}{2\pi}$ magnitude spectrum. The computed output signal $x(t)$ and the unilateral magnitude spectra $2|X(f)|$ are used for our temporal and spectral analyses of VR effect respectively.

Our analyses in this communication mainly focused on how the input low frequency signal $(F\cos\omega t)$ is enhanced at the system output due to presence of high frequency perturbation $(G\cos\Omega t)$. This is studied in the subsequent sections using temporal, spectral, and linear response analyses. Linear response, normally parameterized as Q [14], allows to directly observe how the low frequency signal is enhanced by the high frequency perturbation. Linear response Q is the ratio of the absolute value of the unilateral magnitude spectrum $2|X(f)|$ at the low frequency $f_{Lf} = \frac{\omega}{2\pi}$.to the amplitude of the low frequency signal F

$$Q = \frac{2|X(f_{Lf})|}{F} \qquad (8)$$

Throughout this article, unless otherwise stated, the parameter setting is maintained as: $m = 1, \alpha = 0.19, \omega_0 = 1, \gamma = 0.15, h = 2.0, \omega_p = 2.0,\ \Omega = 10$ as used by S. Roy et al [39] in the same model to control subharmonic resonance and chaos. Moreover, the low frequency signal parameters are fixed to $F = 0.1$ and $\omega = 1$. This setup ensured that the low frequency signal $(F\cos\omega t)$ is subthreshold.

4. RESPONSE OF THE SYSTEM

This section analyses the response of the system to understand how it encodes low frequency signal in the presence of high frequency perturbation. The analyses conducted are mainly temporal and spectral. However, the spectral response is also quantized to better understand the system. Moreover, we studied how the response of the system is controlled by the damping amplitude γ.

4.1. Temporal Analysis

In this section, we study by means of temporal analysis, how the input low frequency signal $F\cos\omega t$ is enhanced at the system output when the perturbation amplitude G varies. Fig. 2 shows the temporal response of the system for three different values of the perturbation amplitude G. The output signal $x(t)$ depicted in each case of Fig. 2 constitutes a low frequency signal and high frequency perturbation. The low frequency signal is represented by the slow oscillations (envelope) while the high frequency signal is represented by the fast oscillations in each case the temporal response of Fig. 2.

For weak perturbation amplitude $G = 20$ depicted in Fig. 2(a), there is weak low frequency contribution in the output signal. Also, for an intermediate value of perturbation amplitude $G = 250$ presented in Fig. 2(b), there is strong low frequency contribution in the output signal. However, for a larger value of perturbation amplitude $G = 450$ depicted in Fig. 2(c), the low frequency contribution in the output signal becomes weak again. Indeed, The best system response is achieved when the perturbation amplitude is tuned to an intermediate value of $G = 250$. This is signifies the VR effect existence in the system.

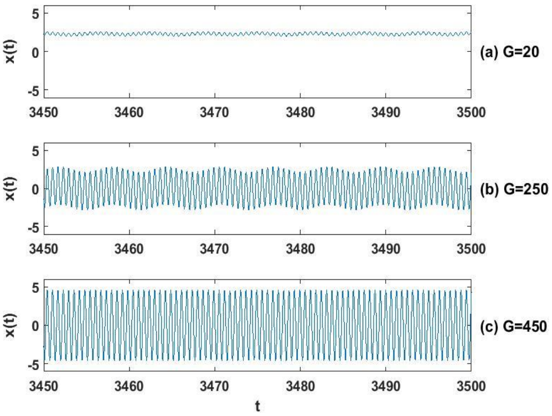

Fig. 2: Temporal response of the system for three values of perturbation amplitude G; (a) G=20, (b) G=250, (c) G=450.

4.2. Spectral Analysis

The temporal analyses demonstration of VR presented Fig. 2 can be equally represented using spectral analyses which provide the better view of VR effect. The unilateral magnitude spectrum $2|X(f)|$ is obtained from the output signal $x(t)$. The unilateral spectra constitute of low frequency spectrum and high frequency spectrum but for convenience, we presented the spectra with the zoom only near the low frequency $\frac{\omega}{2\pi}$. Depicted in Fig. 3 is the unilateral magnitude spectrum with the zoom near the low frequency $\frac{\omega}{2\pi}$ for three different values of the perturbation amplitude G.

For weak perturbation amplitude $G = 20$ depicted in Fig. 3(a), there is weak magnitude spectrum at the low frequency $2|X(f_{Lf})|$. Also, for an intermediate value of perturbation amplitude $G = 250$ presented in Fig. 3(b), there is strong magnitude spectrum at the low frequency $2|X(f_{Lf})|$. However, for larger value of the perturbation amplitude $G = 450$ depicted in Fig. 2(c), the magnitude spectrum at the low frequency $2|X(f_{Lf})|$ becomes weak again. Indeed, the best system response

$2|X(f_{Lf})| = 0.353677$ is achieved when the perturbation amplitude is tuned to an intermediate value of $G = 250$. This signifies the VR effect existence in the system.

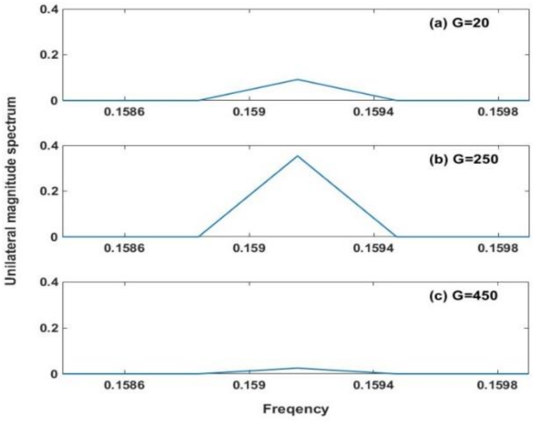

Fig. 3: Spectral response of the system for three values of perturbation amplitude G; (a) G=20, (b) G=250, (c) G=450.

4.3. Quantification of VR Effect

The temporal and spectral analyses revealed VR effect however; the VR phenomenon is best understood by quantifying the spectral response $2|X(f_{Lf})|$. In this section, we quantify VR effect by computing the linear response Q to directly visualize how the low frequency signal is enhanced by varying the perturbation amplitude G. Linear response Q is computed as the ratio of the absolute value of the unilateral magnitude spectrum $2|X(f_{Lf})|$ at the low frequency $f_{Lf} = \frac{\omega}{2\pi}$ to the amplitude of the low frequency F as given by equation (8).

Fig. 4 depicts the linear response Q as a function of the perturbation amplitude G. It can be observed that; varying the perturbation amplitude G, the system revealed two resonances with the last resonance as maximum $Q = 3.5377$ which is achieved for an intermediate value of the perturbation amplitude G. The response of the system is reduced for larger perturbation amplitude beyond the intermediate value. The two resonances revealed by the system may be directly connected with the two potential wells through which the particle attains equilibrium positions. Many studies of VR revealed this kind of typical behavior and it normally attributed to the potential wells. In fact, Usama *et al* [38] also observed multiple resonances in a study of VR in mechanical oscillator with multistable potential wells.

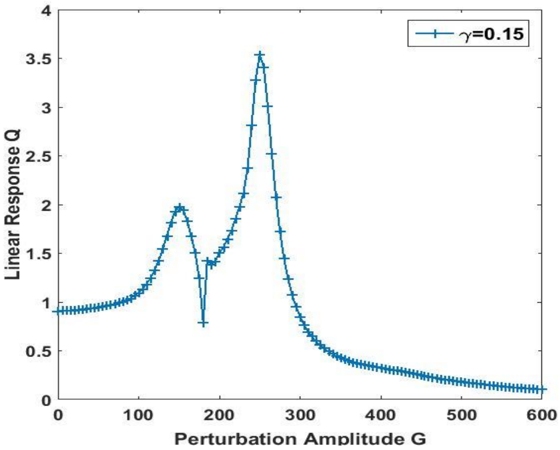

Fig. 4: Linear response Q versus perturbation amplitude G for fixed value of damping amplitude γ=0.15. Parameters setting: m=1, α=0.19, ω_0=1, h=2.0, ω_p=2.0, F=0.1, ω=1, Ω=10.

4.4. Control of VR by Damping Amplitude

In most studies of VR in mechanical systems, VR is controlled by the damping parameters. In the particular model we consider in this paper, we study how damping amplitude γ controls the response of the system.

Presented in Fig. 5 is the linear response Q as a function of the perturbation amplitude G for different value of the damping amplitude γ. Varying the perturbation amplitude G, the system revealed two resonances for each value of the damping amplitude γ. In each case, the second resonance is the global maximum which is achieved for intermediate perturbation amplitude G. The response of the system is reduced when the perturbation amplitude is further increased beyond the intermediate value. Moreover, varying the damping amplitude γ enhances the system's responses but the best response $Q = 7.01557$ is achieved when damping amplitude is tuned to an intermediate $\gamma = 0.05$.

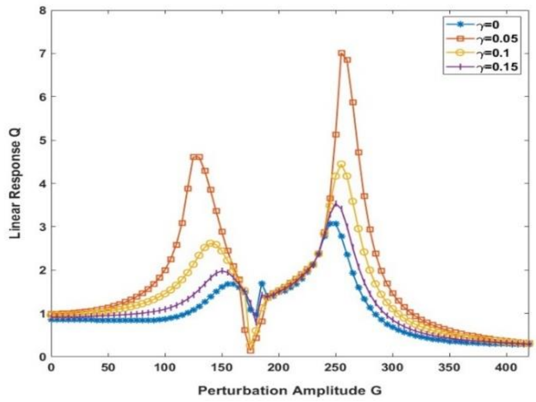

Fig. 5: Linear response Q versus perturbation amplitude G for different values of damping amplitude γ. Parameters setting: m=1, α=0.19, ω_0=1, h=2.0, ω_p=2.0, F=0.1, ω=1, Ω=10.

The case $\gamma = 0$ corresponds to the case when the system is undamped. The response of the undamped system is the minimum response as can be seen from Fig. 5 (with * marker). However, introducing the damping enhances the system's response and the best response is achieved for an intermediate perturbation $\gamma = 0.05$ beyond which the system response reduces again.

5. CONCLUSION

This paper studied subthreshold signal enhancement in a Van der Pol-Duffing oscillator which basically models the motion of a single particle of unit mass in a bistable potential well, experiencing a space-dependent and periodic damping force and driven by an external bichromatic excitation. VR occurrence in the system using temporal and spectral analyses is highlighted. Also, VR effect is highlighted using linear response for a fixed value of the perturbation amplitude. Moreover, the control of VR by the constant damping amplitude γ is also studied.

Indeed, both the temporal and spectral analyses confirmed the occurrence of VR effect in the system. That is, these analyses both depicted how an input low frequency signal is enhanced at the system output due to presence of an intermediate high frequency perturbation. Similarly, the linear response analysis for a fixed value of the damping amplitude highlighted how varying the perturbation amplitude to an intermediate value of $\gamma = 0.05$ enhances the detection of the low frequency signal to $Q = 7.01557$ instead of $Q = 3.5377$ achieved for $\gamma = 0.15$. Moreover the study of the effect of damping amplitude on VR effect has shown that the best system response is achieve for an intermediate damping amplitude γ.

REFERENCES

K. Matsumoto and I. Tsuda. Noise-induced order. J. Stat. Phys., 31(1):87–106, 1983.

A. S. Pikovsky and J. Kurths. Coherence resonance in a noise-driven excitable system. Phys. Rev. Lett., 78:775–778, 1997.

B. Lindner and L. Schimansky-Geier. Coherence and stochastic resonance in a two-state system. Phys. Rev. E, 61(6):6103, 2000.

P. K. Shaw, D. Saha, S. Ghosh, M. S. Janaki, and A. N. S. Iyengar. Intrinsic noise induced coherence resonance in a glow discharge plasma. Chaos, 25(4):043–101, 2015.

O. V. Ushakov, H. J. Wünsche, F. Henneberger, I. A. Khovanov, L. Schimansky-Geier, and M. A. Zaks. Coherence resonance near a Hopf bifurcation. Phys. Rev. Lett., 95:123903, 2005.

V. Beato, I. Sendina-Nadal, I. Gerdes, and H. Engel. Coherence resonance in a chemical excitable system driven by coloured noise. Philos. Trans. Royal Soc. A, 366(1864):381–395, 2007.

R. Benzi, G. Parisi, A. Sutera, and A. Vulpiani. Stochastic resonance in climatic change. Tellus, 34(1):10–16, 1982.

L. Gammaitoni, P. Hänggi, P. Jung, and F. Marchesoni. Stochastic resonance: a remarkable idea that changed our perception of noise. Eur. Phys. J. B, 69(1):1–3, 2009.

F. Duan, F. Chapeau-Blondeau, and D. Abbott. Encoding efficiency of suprathreshold stochastic resonance on stimulus-specific information. Phys. Lett. A, 380(1-2):33–39, 2016.

Y. Ren, Y. Pan, F. Duan, F. Chapeau-Blondeau, and D. Abbott. Exploiting vibrational resonance in weak-signal detection. Phys. Rev. E, 96(2):022141, 2017.

Y. Pan, F. Duan, F. Chapeau-Blondeau, and D. Abbott. Noise enhancement in robust estimation of location. IEEE Trans. Signal Process., 66(8):1953–1966, 2018.

N. Gillard, É. Belin, and F. Chapeau-Blondeau. Stochastic resonance with unital quantum noise. Fluct. Noise Lett., 18(03):1950015, 2019.

F. Duan, L. Duan, F. Chapeau-Blondeau, Y. Ren, and D. Abbott. Binary signal transmission in nonlinear sensors: Stochastic resonance and human hand balance. Instru. Meas. Mag., 23(1):44–49, 2020.

P. S. Landa and P. V. E. McClintock. Vibrational resonance. J. Phys. A, 33(45):L433, 2000.

E. Ullner, A. Zaikin, J. García-Ojalvo, R. Bascones, and J. Kurths. Vibrational resonance and vibrational propagation in excitable systems. Phys. Lett. A, 312(5-6):348–354, 2003.

L. Ning and Z. Chen. Vibrational resonance analysis in a gene transcriptional regulatory system with two different forms of time-delays. Physica D, 401:132164, 2020.

B. I. Usama, S. Morfu, and P. Marquié. Vibrational resonance and ghost-vibrational resonance occurrence in Chua’s circuit models with specific nonlinearities. Chaos Solitons Fract., 153, pp.11151, 2021.

H. Shengping, J. Zhang, J. Yang, H. Liu, and M. A. F. Sanjuán. Logical vibrational resonance in a symmetric bistable system: Numerical and experimental studies. Commun Nonlinear Sci. Numer. Simul., 119:107123, 2023.

D. R. Chialvo, O. Calvo, D. L. Gonzalez, O. Piro, and G. V. Savino. Subharmonic stochastic synchronization and resonance in neuronal systems. Phys. Rev. E, 65(5):050902, 2002.

M. Bordet, S. Morfu, and P. Marquié. Ghost responses of the FitzHugh–Nagumo system induced by colored noise. Chaos, Solitons Fract., 78:205–214, 2015.

S. Rajamani, S. Rajasekar, and M. A. F. Sanjuán. Ghost-vibrational resonance. Commun Nonlinear Sci. Numer. Simul., 19(11):4003–4012, 2014.

K. Abirami, S. Rajasekar, and M. A. F. Sanjuán. Vibrational resonance in a harmonically trapped potential system. Comm. Nonlinear Sci. Numer. Simulat., 47:370–378, 2017.

F. Duan, F. Chapeau-Blondeau, and D. Abbott. Stochastic resonance with colored noise for neural signal detection. PLoS One, 9(3):e91345, 2014.

Y. Ren, Y. Pan, F. Duan, F. Chapeau-Blondeau, and D. Abbott. Exploiting vibrational resonance in weak-signal detection. Phys. Rev. E, 96(2):022141, 2017.

N. Gillard, É. Belin, and F. Chapeau-Blondeau. Stochastic antiresonance in qubit phase estimation with quantum thermal noise. Phys. Lett. A, 381(32):2621–2628, 2017.

N. Gillard, É. Belin, and F. Chapeau-Blondeau. Enhancing qubit information with quantum thermal noise. Physica A, 507:219–230, 2018.

A. Delahaies, F. Chapeau-Blondeau, D. Rousseau, and F. Franconi. Tuning the noise in magnetic resonance imaging to maximize nonlinear information transmission. Fluct. Noise Lett., 12(01):1350005, 2013.

L. Duan, F. Duan, F. Chapeau-Blondeau, and D. Abbott. Stochastic resonance in Hopfield neural networks for transmitting binary signals. Phys. Lett. A, 384(6):126–143, 2020.

V. N. Chizhevsky. Experimental evidence of vibrational resonance in a multistable system. Phys. Rev. E, 89(6):062914, 2014.

S. Morfu and M. Bordet. On the correlation between phase-locking modes and vibrational resonance in a neuronal model. Commun Nonlinear Sci. Numer. Simul., 55:277–286, 2018.

T. O. Roy-Layinde, J. A. Laoye, O. O. Popoola, U. E. Vincent, and P. V. E. McClintock. Vibrational resonance in an inhomogeneous medium with periodic dissipation. Phys. Rev. E, 96(3):032209, 2017.

V. N. Chizhevsky. Amplification of an autodyne signal in a bistable vertical-cavity surface emitting laser with the use of a vibrational resonance. Tech. Phys. Lett., 44(1):17–19, 2018.

S. Morfu, B. I. Usama, and P. Marquié. Perception enhancement of subthreshold noisy image with vibrational resonance. Electron. Lett., 2019.

T. O. Roy-Layinde, K. A. Omoteso, O. Kolebaje, F. O. Ogunmefun, R. A. Fasasi, J. A. Laoye, and U. E. Vincent. Vibrational resonance in a multistable system with position-dependent mass. Commun. Theor. Phys., 75(11): 115602, 2023.

K. S. Kannan, S. M. Abdulkader, V. Chinnathambi, M.V. Meenakshi, S. Rajasekar. Nonlinear resonance in a position-dependent mass-Duffing oscillator system with monostable potentials driven by an amplitude-modulated signal. Russian journal. Of nonlinear dynamics, 9(3): 389-408, 2023.

B. I. Usama, H. Mustapha, and G. S. Shehu. Subthreshold signal detection and enhancement in Duffing oscillator via vibrational resonance. Nigerian Journal of Engineering. 27(3): 23-27, 2020.

R. Kabilan, A. Venkatesan. Vibrational resonance in a damped bi-harmonic driven Mathews-Lakshmanan oscillator. Journal of Vibration Engineering & Technology. 12(1):1123-1131, 2024.

B. I. Usama, S. Morfu, and P. Marquié. Numerical analyses of the vibrational resonance occurrence in a nonlinear dissipative system. Chaos Solitons Fract., 127:31–37, 2019.

S. Roy, A. Ray, A. Roy chowdhury. Controlling sub-harmonic resonance and chaos by a fast forcing in a Van der Pol-Duffing oscillator with parametrically excited damping. Chaos Solitons Fract.,174: 113857, 2023.